Tuning thermoelectric performance of *π-d* conjugated nickel coordination polymers through metal−ligand frontier molecular orbital alignment

Yong etc.

ABSTRACT

π-d conjugated transition-metal coordination polymers have been rapidly emerging as one of the most attractive polymer-based thermoelectric materials in the past decade. However, few studies have elucidated the relation between their geometric structures, orbital characteristics, and thermoelectric properties, which has seriously hindered the development of a straightforward design strategy for *π-d* conjugated polymer-based thermoelectric materials. Herein, taking poly(nickel-benzene-1,2,4,5-tetrathiolate) and its derivatives as specimen models, we have studied the effect of ligand chemical modulation on the thermoelectric properties and elucidated structure-property relationships based on the first-principles calculations. Our theoretical results indicate that thermoelectric power factor is governed by the frontier molecular orbital alignment between the square planar metal-tetrasulfide fragment and the organic π-conjugated spacers. Specifically, a better frontier molecular orbital alignment results in weaker the electron-phonon coupling. Consequently, higher mobility can be achieved, which leads to higher thermoelectric power factor. This finding provides a screening rule for the rationalization and design of high performance p-type *π-d* conjugated transition-metal coordination thermoelectric polymers.

Introduction

Thermoelectric (TE) materials, which enable direct interconversion of heat and electricity *via* the Seebeck or Peltier effects, play an important role in meeting the world's growing energy demand.[1][2] The efficiency of a TE material is characterized by the dimensionless figure of merit: $zT = S^2\sigma T/\kappa$, where S, σ, κ, and T represent Seebeck coefficient, electrical conductivity, total thermal conductivity including the electronic and lattice thermal conductivities, and absolute temperature, respectively. These parameters (S, σ, and κ) are mutually coupled, making it extraordinarily difficult to achieve a high zT in a straightforward manner.[3] For example, an increase in electrical conductivity would be accompanied by an increase in electronic thermal conductivity, and a decrease in Seebeck coefficient. A favorable scenario for a high TE performance material is the simultaneous presence of a high Seebeck coefficient and electrical conductivity, and a low thermal conductivity. Currently, the most successful strategies to elevate the zT include engineering the band structures, e.g. high band degeneracy and resonant states, and suppressing the lattice thermal conductivity, which can be realized in one material.[4]–[6]

Conducting polymers have triggered a renewed interest in their applications as TE materials due to their unique properties like light-weight, high flexibility, solution processability, and low cost.[7]–[9] In the past decade, a variety of high-performance polymeric TE materials, including π-conjugated polymers,[10][11] organic-inorganic composites,[12]–[14] and *π-d* conjugated transition-metal coordination polymers[15][16] have emerged. Among them, *π-d* conjugated transition-metal coordination polymers have attracted increasing attention[8][15][16] due to their outstanding TE performance. For examples, poly(Ni-ethylenetetrathiolate)), (**Ni-ETT**) powder[15] was initially found to have a zT value of 0.2 at 400 K, with an electrical conductivity of ~ 60 S cm^{-1}, a Seebeck coefficient of ~ -150 μV/K, and a small thermal conductivity of 0.25 W m^{-1} K^{-1}. Later, the zT value of **Ni-ETT** film[16] was further improved to 0.4 at 400 K with an enhanced electrical conductivity of ~ 220 S cm^{-1}, the same Seebeck coefficient of ~ -150 μV/K, and a similar poor thermal conductivity of 0.82 W m^{-1} K^{-1}. Poly(Ni-benzene-1,2,4,5-tetrathiolate), **Ni-BTT** and its derivatives is another class of successfully synthesized *π-d* conjugated nickel coordination polymers with extremely high electrical conductivity exceeding 800 S cm^{-1} at room temperature.[17][18] In comparison to the significant progress in enhancing the transport properties of coordination polymers, few studies have elucidated the relation between the geometric structures, orbital

characteristics, and thermoelectric properties of these materials. This has seriously hindered experimentalists' efforts to explore new *π-d* conjugated polymer-based thermoelectric materials.

In this work, based on density functional theory (DFT) calculations and Boltzmann transport theory, we have investigated the structure-property relationship of p-type **Ni-BTT** and its five derivatives. Our calculations have revealed that good frontier molecular orbital alignment between the square planar nickel-tetrasulfide fragment and the organic π-conjugated spacer is a strong predictor of high TE performance for a coordination polymer. Specificly, a good frontier molecular orbital alignment results in strong *p-d* coupling between the square planar nickel-tetrasulfide fragment and the organic π-conjugated spacer, which suppresses electron-phonon couplings. Consequently, higher mobility can be achieved, which leads to higher thermoelectric power factor. This finding provides a screening rule to aid experimentalist in designing new high-performance p-type *π-d* conjugated transition-metal coordination TE polymers.

Computational methodology

Geometrical and electronic structure calculations.

In present work, we use isolated polymer chains to explore the intrinsic intra-chain TE properties. The periodic direction of the infinite polymer chain is defined as the *x* axis. (Figure 1a). A 20 Å vacuum is set up for each polymer chain above the perpendicular y and *z* directions. Both lattice parameters and atomic positions were optimized. First, different functionals including LDA, LDA+U, PBE[19], PBE+U, and HSE06[20] with the Grimme's DFT-D3 van der Waals dispersion corrections[21] were evaluated for geometrical optimizations and electronic structure calculations. The detailed calculation results are given in Section I in the Supporting Information (SI). PBE and HSE06 produced almost the same lattice constants and bond lengths, which reproduced the experimental structural parameters better than LDA and LDA+U functionals. LDA+U, PBE, and PBE+U calculations gave metallic band structures (Figure S2) for **Ni-BTT**, but the HSE06 calculated band structure is semiconducting with a small band gap around 0.08 eV which is consistent with experimental observations.[22] However, the band profiles obtained by PBE+U (U = 6.0 eV) and HSE06 functional are nearly the same. Thus, considering the balance between accuracy and computational cost, PBE functional with van der Waals dispersion corrections was employed for the geometry optimizations and a 16×1×1 k-point mesh was used for Brillouin zone

sampling. HSE06 functional with van der Waals dispersion corrections was used to conduct the electronic structure calculations, with a 20×1×1 k-point mesh for Brillouin zone sampling. All calculations were performed using Vienna ab Initio Simulation Package (VASP) code,[23]–[26] employing projector-augmented wave (PAW)[27] and plane wave basis set for C, S, and Ni atoms with cut-off energy of 600 eV.

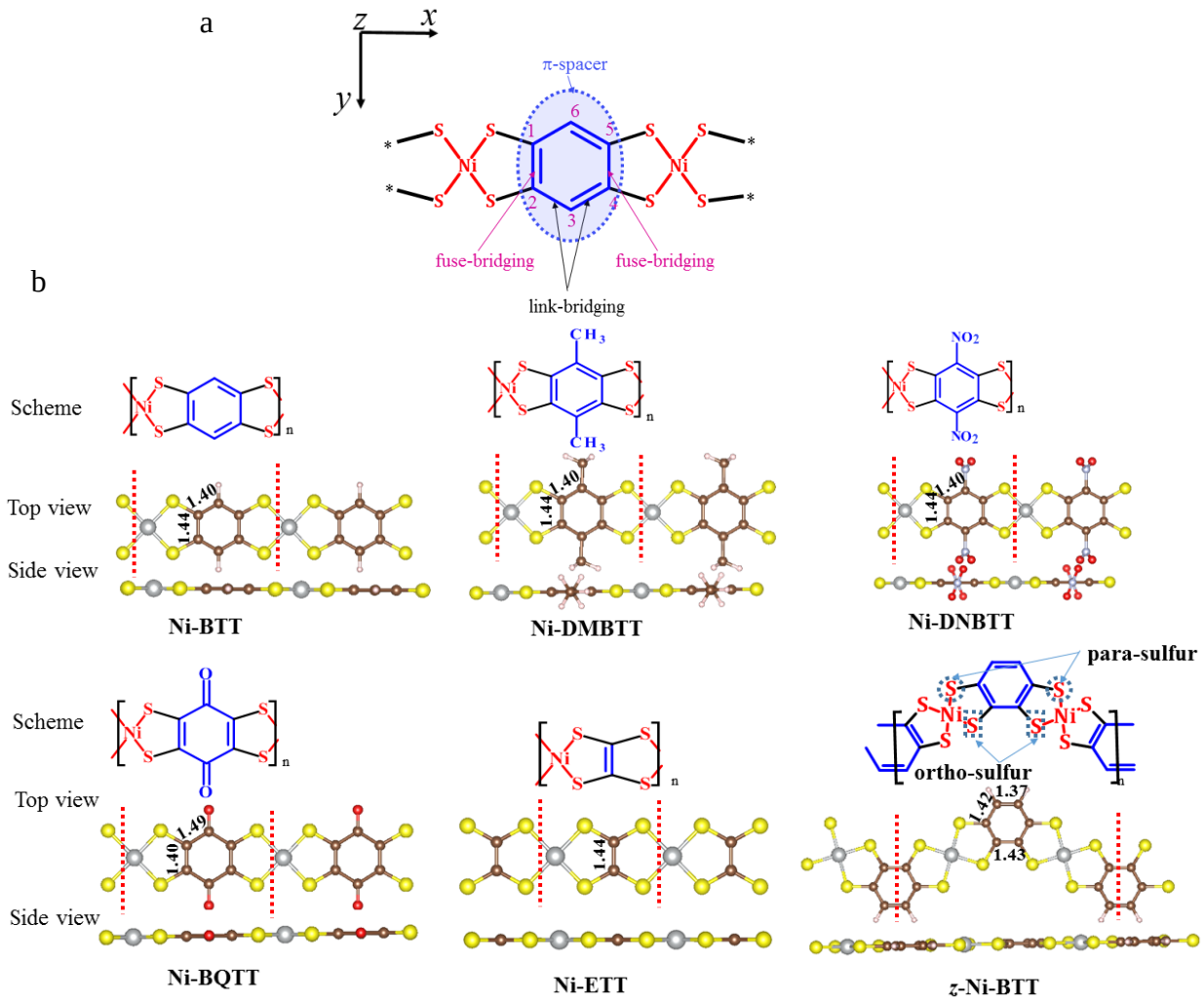

Figure 1. Chemical structures. (a) Schematic illustration of the polymer backbone and the definitions of square planar nickel-tetrasulfide fragment (in red) and organic π-conjugated spacer (in blue) as well as the fuse-bridging and link-bridging C-C bonds within the aromatic π-conjugated spacer with the numbering of C atoms labeled. For the ease of understanding, the C-C bonds in the benzene-like π-conjugated spacer are grouped into two types: fuse-bridging bonds (C1-C2, and C4-C5 in **Ni-BTT**, C1-C2, and C3-C4 in ***z*-Ni-BTT**, perpendicular to the polymer

backbone) and link-bridging bonds (C2-C3, C3-C4, C1-C6, C5-C6 in **Ni-BTT**, C2-C3, C4-C5, and C5-C6 in ***z*-Ni-BTT**, along the polymer backbone). (b) Optimized chemical structures with top and side views for **Ni-BTT**, **Ni-DMBTT**, **Ni-DNBTT**, **Ni-BQTT**, **Ni-ETT**, and ***z*-Ni-BTT**. The selected C-C bond lengths are labeled on the optimized structures. The optimized structural pentamers for **Ni-BTT** are given in Figure S1.

TE transport coefficients calculations. The electrical conductivity, σ and Seebeck coefficient, S are obtained by solving the Boltzmann transport equation expressed as:

$$\sigma = \frac{e^2}{V}\sum_k(-\frac{\partial f_0(\epsilon_k)}{\partial \varepsilon_k})v_k v_k \tau_k, \quad (1)$$

$$S = \frac{e}{V\sigma T}\sum_k(-\frac{\partial f_0(\epsilon_k)}{\partial \varepsilon_k})(\varepsilon_k - \varepsilon_F)v_k v_k \tau_k. \quad (2)$$

Here, $f_0(\varepsilon_F) = 1/(\exp^{(\varepsilon_k - \epsilon_F/k_B T)} + 1)$ is the Fermi-Dirac distribution function, τ_k, ε_F, V, and v_k represent the relaxation time, Fermi energy level, volume, and group velocity, respectively. To estimate the summation in the k-space, we applied Wannier function-based interpolation techniques to obtain the ultra-dense band energies via the wannier90 program.[28] The TE properties were calculated by BoltzTrap program.[29][30] According to Fermi's Golden rule, relaxation time, $\tau_{\boldsymbol{k}}$ is obtained via the formula $1/\tau_{\boldsymbol{k}} = (2\pi/\hbar)\sum_{\boldsymbol{k}'}|M(\boldsymbol{k},\boldsymbol{k}')|^2\delta(\varepsilon_{\boldsymbol{k}} - \varepsilon_{\boldsymbol{k}'})(1-\cos\theta)$, Here $\hbar$ is the reduced Planck constant, $\delta(\varepsilon_{\boldsymbol{k}} - \varepsilon_{\boldsymbol{k}'})$ is the Dirac delta function, θ is the scattering angle between $\boldsymbol{k}$ and $\boldsymbol{k}$' states, and ***M(k,k')*** is the scattering matrix element. In this work, the electron-phonon scattering matrix element is modeled from deformation potential (DP) theory,[31] which has the form, $M(\boldsymbol{k},\boldsymbol{k}') = ({E_1}^2/C_{ii})k_B T$, where E_1 is the DP constant and C_{ii} is the elastic constant. The detailed calculation methods for DP constants and elastic constants can be found in Section-III in SI.

Results and discussion

Polymer backbone structure

Each *π-d* conjugated nickel coordination polymer (Figure 1) can be described as a square planar nickel-tetrasulfide fragment linked by π-conjugated organic spacers (Figure 1a). When nickel-tetrasulfide is linked with the benzene π-conjugated spacer, two polymeric conformations can be obtained, *i.e.*, a linear **Ni-BTT** and a zigzag poly(Ni-1,2,3,4-tetrathiolate), ***z*-Ni-BTT** (Figure 1b). By modulating benzene with different functional groups, we investigated three additional linear

coordination polymers, named as poly(Ni-3,6-dimethylbenzenetetrathiolate), (**Ni-DMBTT**, electron donating groups, -CH_3), poly(Ni-3,6-dinitrobenzene-1,2,4,5-tetrathiolate (**Ni-DNBTT**, electron withdrawing groups, -NO_2), and poly(Ni-3,6-benzoquinone-1,2,4,5-tetrathiolate) (**Ni-BQTT)**. **Ni-ETT** contains the ethylene as the organic spacer. Among these six polymers, **Ni-BTT**[18] and **Ni-ETT**[15][16] have been successfully synthesized. While the other four are proposed structures are not yet known, they are synthetically feasible.

All optimized polymers possess a planar ladder-like structure as shown in Figure 1 where the nickel-tetrasulfide fragment remains square planar due to the dsp^2 hybridization of the nickel atoms. The binding of the organic π-conjugated spacers to the nickel-tetrasulfide fragment allow no rotation in the structure facilitating the extension of the electron conjugation along the polymer chains (Figure 1) and is in favor of good intra-chain charge transport properties. All of these six coordination polymers have similar Ni-S and C-S bond lengths (Ni-S: 2.14 – 2.16 Å, C-S: 1.69 – 1.71 Å, see Table S1 in SI) which are comparable to those in solid **Ni-ETT** deduced from extended X-ray absorption fine structure analysis[15] and those of nickel-benzene-tetrathiolate anions obtained from X-ray powder diffraction.[32] The main differences are in the C-C bond length alternations within the aromatic π-conjugated spacer. In **Ni-BTT**, the fuse-bridging C-C bonds are around 1.44 Å, and the link-bringing C-C bonds are around 1.40 Å (Figure 1). Compared to **Ni-BTT**, the D_{2h} symmetry disappears in ***z*-Ni-BTT**. One of the link-bridging C-C bonds in ***z*-Ni-BTT** is shortened to a C=C double bond (1.37 Å) (Figure 1b), indicating the electron density is localized, leading to loss of electronic conjugation. Introducing electron-donating (**Ni-DMBTT**) or electron withdrawing groups (**Ni-DNBTT**) brings little structural changes (Figure 1 and Table S1) compared to **Ni-BTT**. However, when quinone is used as organic spacers (**Ni-BQTT**), the C-C bond length alternations changes significantly, while the Ni-S and C-S remain similar to those in **Ni-BTT**. The fuse-linking C-C bonds in **Ni-BQTT** are shorter (1.40 Å) than the link-bridging C-C bonds (1.49 Å) with the link-bridging C-C bonds showing significant single bond character. Hence, **Ni-DMBTT** and **Ni-DNBTT** are expected to have a similar degree of electron conjugation compared with **Ni-BTT**, while **Ni-BQTT** and ***z*-Ni-BTT** may have a weaker degree of electron conjugation.

Electronic structure characteristics.

The bandwidth and effective mass for a TE material are the two critical quantities which affect the intrinsic charge transport and TE properties. Herein, we investigate how different organic π-spacers affect the band structures (Figure 2 and Figure S4) of the coordination polymers. To obtain insight into structural effects, we plot the atomic orbital component ratios within the whole valence band (VB) (Figure 3) including the p_z orbitals of S atoms, d_{xz} orbitals of Ni atoms, and p_z orbitals of the C atoms in the aromatic rings and O, N, and C atoms in the functional groups of the aromatic spacers. **Ni-BTT** and **Ni-ETT** have similar VB bandwidths of ~ 1.78 eV (Table S2) but different orbital component ratios. The VB of **Ni-ETT** is mainly composed of the nickel-tetrasulfide fragment, where d_{xz} orbitals of Ni atom and the p_z orbitals of S atoms contribute approximately 66% and 30%, respectively, with the remaining 4% from the p_z orbitals of C atoms of the π-conjugated spacer. For **Ni-BTT**, the orbital contribution to VB from π-conjugated spacer increases but from nickel-tetrasulfide fragment decreases. The p_z orbitals of C atoms in the π-spacer, d_{xz} orbital of Ni atom, p_z orbital of the S atoms contribute 25%, 28% and 47% to VB, respectively. At the valence band maximum (VBM) of **Ni-BTT** (Figure 2b), the partial charge distributes solely on S (p_z) and C (p_z) atoms of the fuse-bridging C-C bond of the π-spacer. In contrast the partial charge for the VBM of **Ni-ETT** distributes solely on the Ni (d_{xz} orbitals) atoms and S (p_z) atoms. The VBM and CBM (conduction band minimum) of **Ni-BTT** are lower in energy than those of **Ni-ETT** by 0.36 eV and 1.33 eV respectively. Therefore, **Ni-BTT** has a smaller band gap (0.08 eV) as compared with **Ni-BTT** (1.05 eV).

When electron-withdrawing or electron-donating groups are introduced at the 3,6 para positions of the benzene ring, little changes occur in the band structures for **Ni-DNBTT** and **Ni-DMBTT** compared with that of **Ni-BTT**. Both VB bandwidths (1.68 eV for **Ni-DNBTT** and 1.80 eV for **Ni-DMBTT**), and band gap (0.10 eV for **Ni-DNBTT** and 0.08 eV for **Ni-DMBTT**) remain similar to **Ni-BTT**. Similarly, little change is found in the orbital component ratios in VB compared with that of **Ni-BTT**; and d_{xz} (Ni), p_z (S) and p_z (C) contribute about 25 – 26%, 50 – 52% and 25 – 27% to VB, respectively. In addition, the functional groups do not directly affect in the partial charge distributions of VBM (Figure 2c-d). Therefore little changes occur in band structures. The introduction of electron withdrawing or donating groups mainly produces a rigid down- or up-ward-shift in the VBM and CBM energy levels compared to **Ni-BTT**, respectively. In addition, the electron-donating/withdrawing amounts of -CH_3/-NO_2 groups are characterized with the bader

charge analysis where the -CH_3 (-NO_2) group is found to lose (gain) 0.21e (0.47e) as summarized in Table S3. The band structure of **Ni-BQTT** (Figure 2e) shows dramatic changes. The VB bandwidths decrease from 1.78 eV in **Ni-BTT** to 0.78 eV in **Ni-BQTT**, because the link-bridging C-C bonds are almost single bonds and attenuate the π-*d* and *p*-*p* conjugations. The energies of VBM and CBM of **Ni-BQTT** shift down by 0.79 eV and 0.09 eV respectively compared with those of **Ni-BTT**; the band gap is enlarged to 0.78 eV compared with **Ni-BTT** (0.08eV).

***z*-Ni-BTT** also shows a fairly different band structure (Figure S4) and its VB bandwidth narrows down to 0.14 eV from 1.78 eV of **Ni-BTT**. Apart from the formation of a localized C=C double bond as described above in the geometry optimization section, the zigzag conjugation breaks the D_{2h} symmetry, and the four S coordination atoms are not chemically degenerated. As a result, the partial charge at VBM only distributes on the para sulfur atoms and the fuse-bridging C-C bonds (Figure S4), implying that orbital conjugation between para sulfur atoms and the fuse-bridging C-C bonds would be the sole hole conductive channel[33] and ***z*-Ni-BTT** is detrimental for hole transport. Due to poor conjugation, the VBM (CBM) of ***z*-Ni-BTT** is higher in energy by 0.45 eV (1.11 eV) than that of **Ni-BTT**. Consequently, the band gap of ***z*-Ni-BTT** (0.74 eV) is larger than that of **Ni-BTT** (0.08 eV).

The hole effective mass, m^* of the five linear coordination polymers studied in this work are in the range of 0.040 – 0.313m_e (Figure 3b), and such small effective mass is in favorer of excellent hole transport properties. Experimentally, cyclopenta [2,1-b:3,4-b']dithiophene pyridyl[2,1,3]-thiadiazole (PCDTPT) is identified as a typical hole-transport polymer with a measured hole effective mass of 0.106m_e along the intra-chain direction using angle-resolved photoemission spectroscopy.[34] Our calculated hole effective mass for **Ni-BTT** (0.105m_e) is very close to that of PCDTPT, while the m^* of **Ni-DMBTT** (0.022m_e) and **Ni-DNBTT** (0.040m_e) are one magnitude smaller. However, the hole effective mass of **Ni-ETT** (0.244m_e) and **Ni-BQTT** (0.312m_e) are found to be 2 - 3 times larger than that of PCDTPT. In addition, a trend of increasing effective mass with widening band gap of the coordination polymer is observed which agrees well with our previous work.[35]

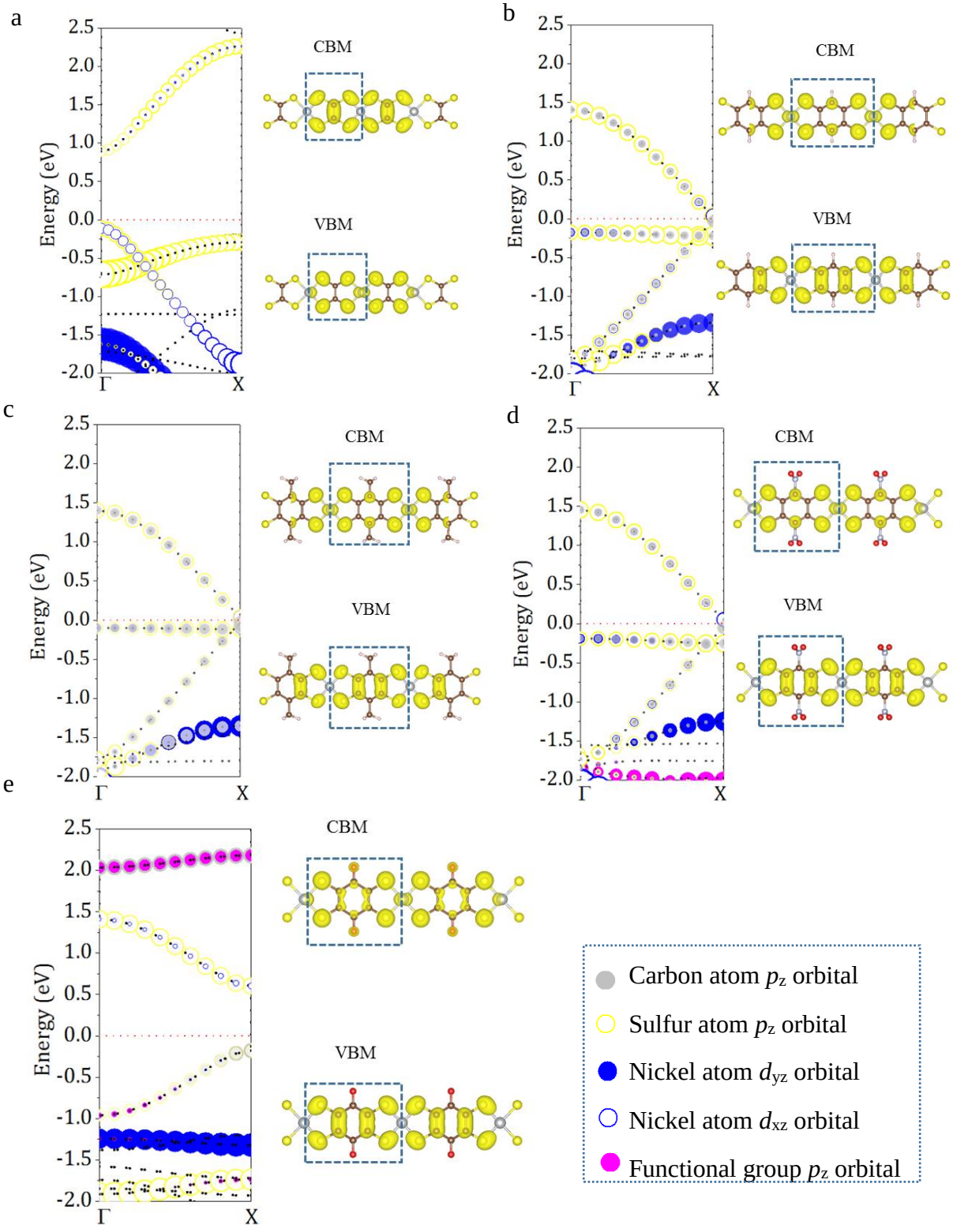

Figure 2. The orbital-projected band structures and partial charge distributions of VBM and CBM for (a) **Ni-ETT**, (b) **Ni-BTT**, (c) **Ni-DMBTT**, (d) **Ni-DNBTT**, and (f) **Ni-BQTT** respectively. The

symbol sizes correspond to the relative weights. The non-orbital-projected band structures are displayed in black dashed lines, and red dashed lines represent Fermi levels. The reciprocal coordinates of high-symmetry k-points in the first Brillouin zone are Γ = (0, 0, 0) and X = (0.5, 0, 0).

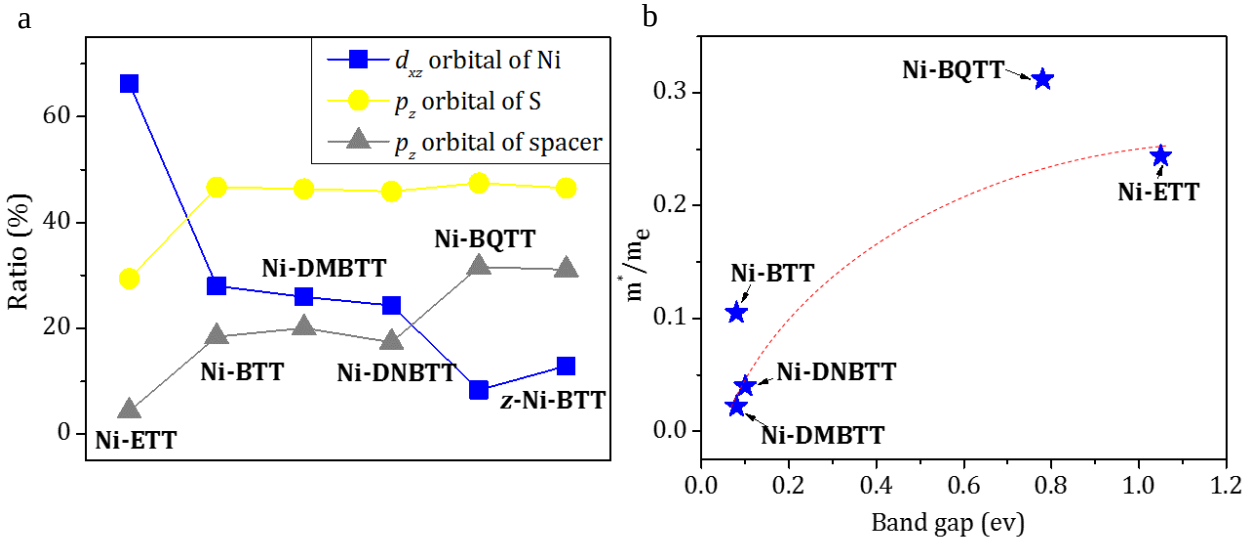

Figure 3. VBM characters. (a) The atomic orbital component ratios contribute to the whole valence bands of the six coordination polymers including the d_{xz} orbital of Ni atoms, p_z orbital of S atoms, and p_z orbitals of the C atoms of the aromatic rings and O, N, and C atoms of the functional groups in spacers. (b) The relation between hole effective mass, m^*/m_e and the band gap of the coordination polymers.

Electron-phonon coupling.

The electron-phonon coupling is an important factor which governs the intrinsic charge transport. We have reported that the low-energy acoustic phonon modes play a dominant role in electron scattering for *π-d* conjugated transition-metal coordination polymers with similar structural motif.[35] Accordingly, in this work, the acoustic phonon scatterings are taken into account within DP theory,[31] where DP constants, E_1, and elastic constants, C_{ii}, are the two pivotal physical quantities used to describe electron-acoustic phonon coupling.

As shown in Figure 4b, the E_1 for holes adopts varying values across the coordination polymers with different π-conjugated spacers. The corresponding data are summarized in Table S4. The E_1 for the holes of **Ni-ETT** (4.45 eV) is much larger than those of the linear coordination polymers with aromatic π-conjugated spacers (0.12 – 1.28 eV). In comparison, the measured E_1 for $CH_3NH_3PdI_3$ is 2.93 eV[36] for a high mobility of 2800 $cm^2\ V^{-1}\ s^{-1}$ using the coherent acoustic phonons generated by femtosecond laser pulses technique. Among the coordination polymers, although the calculated E_1 of **Ni-ETT** is much larger than that of $CH_3NH_3PdI_3$, the E_1 of linear coordination polymers with aromatic π-conjugated spacers are much smaller than that of CH3NH3PdI3, implying potentially high intrinsic mobility.

An interesting finding is that E_1 for the coordination polymers increases with better frontier molecular orbital alignment between the square planar nickel-tetrasulfide fragment and the organic π-conjugated spacer. Specifically, as shown in Figure 4b, the E_1 is found to vary with the increment of $\Delta\varepsilon$, which is employed to characterize the molecular orbital alignment and defined by,

$$\Delta\varepsilon = \mathrm{abs}[E_{HOMO}(NiS_4) - E_{HOMO}(spacer)]. \quad (3)$$

Here, $E_{HOMO}(NiS_4)$ and E_{HOMO}(spacer) are the highest occupied molecular orbital (HOMO) energy levels of the square planar nickel-tetrasulfide isolated fragment and organic π-spacer, respectively. Δε takes the absolute value and a smaller Δε is considered as a better frontier molecular orbital alignment (Figure 4a). Benzene and square planar nickel-tetrasulfide fragment have the best frontier molecular orbital alignment with a small $\Delta\varepsilon$ of 0.12 eV (Figure 4a), resulting in the smallest E_1 for **Ni-BTT** (0.12 eV). The inclusion of electron donating/withdrawing groups produces an up/down-shift in the HOMO of the isolated fragments. Therefore, the HOMOs of 1,4-dinitrobenzene and 1,4-dimethylbenzene are shifted away from the HOMO of square planar nickel-tetrasulfide fragment, leading to Δε of 1.73 eV and 0.54 eV, respectively, (Figure 4a). As a result, the E_1 of the corresponding coordination polymers **Ni-DNBTT** (1.04 eV) and **Ni-DMBTT** (0.29 eV) are larger than that of **Ni-BTT** (0.12 eV). For 1,4-benzoquinone, as compared with benzene, the electronegative O atoms tend to lower the HOMO while its quinoid-structure has an upward-shift effect on the HOMO due to poorer electron conjugation. The overall effect helps the 1,4-benzoquinone to have a comparably good alignment with square planar nickel-tetrasulfide fragment with the Δε of only 0.89 eV, leading to a small E_1 for **Ni-BQTT** (0.24 eV). Ethylene has

the weakest alignment with square planar nickel-tetrasulfide fragment with a large $\Delta\varepsilon$ (2.73 eV). Thus, **Ni-ETT** has the largest E_1 (4.45 eV). Therefore, these results reveal that the $\Delta\varepsilon$ plays a dominant role in electron-phonon coupling for this series of coordination polymers. A better frontier molecular orbital alignment gives rise to a smaller E_1, which indicates smaller electron-phonon coupling.

The E_1 of holes for the ***z*-Ni-BTT** (1.28 eV) is much larger than that of linear **Ni-BTT** (0.28 eV). Such difference can be partially understood from the fuse-bridging C-C bond deformations. The deformation of fuse-bridging C-C bonds (0.14% Figure S8) in ***z*-Ni-BTT** is seven times larger than those in **Ni-BTT** (0.02% Figure S8); such strong deformation perpendicular to the crystal orbitals has been shown to induce large E_1.[38]

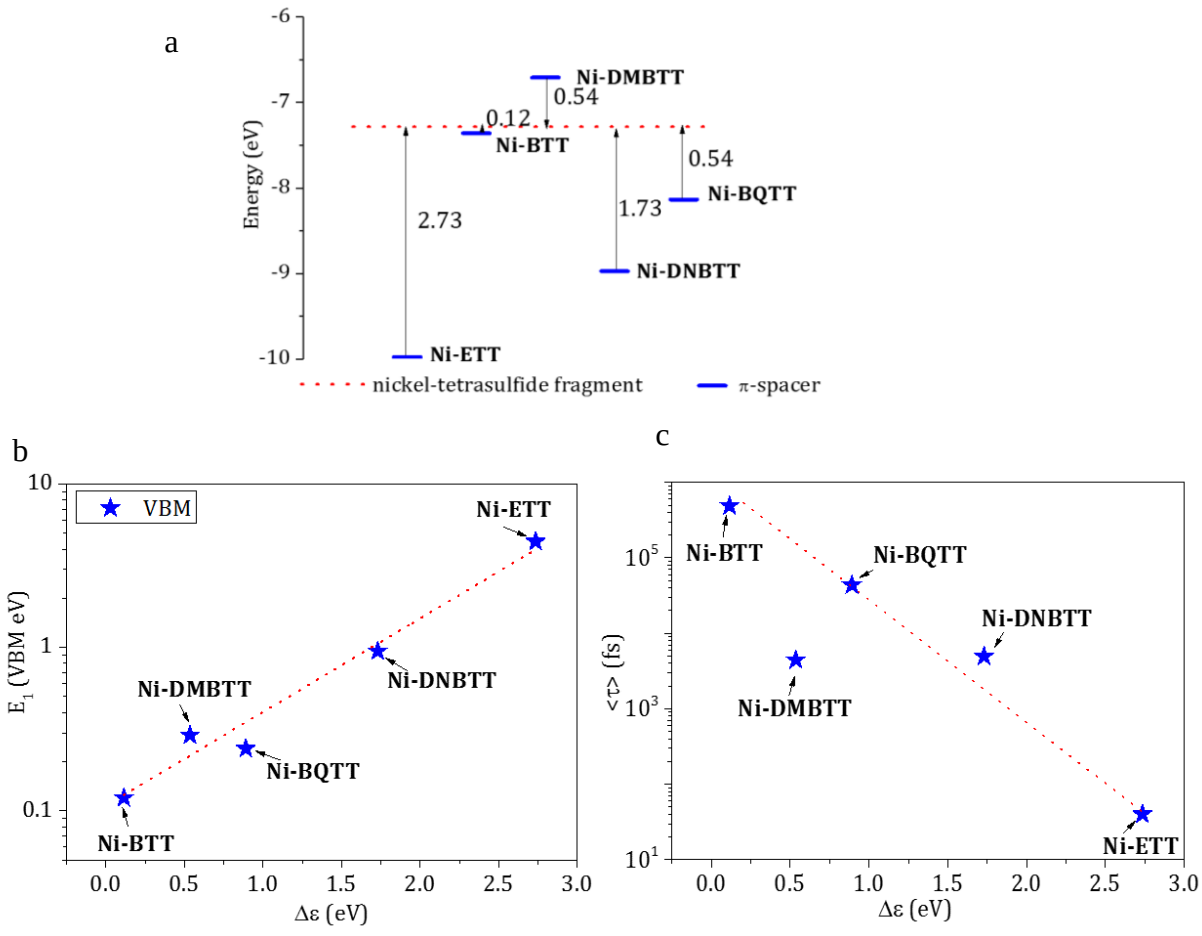

Figure 4. Electron-phonon couplings *vs.* frontier molecular orbital alignment between the square planar nickel-tetrasulfide fragment and the π-conjugated spacer which comprises the coordination polymers. (a) The frontier orbital alignment is represented by the absolute energy difference, $\Delta\varepsilon$ between the HOMOs of the isolated molecular fragments. The value of $\Delta\varepsilon$ for each coordination polymer is labeled. (b) The trend of the electron DP constants of the VBM, E_1 *vs.* the absolute value of the energy difference $\Delta\varepsilon$. The red dotted line represents the increasing trend of DP constantans with increasing $\Delta\varepsilon$. (c) The trend of the mean electron relaxation times, $\langle\tau\rangle$ *vs.* $\Delta\varepsilon$ at 298 K. The logarithmic E_1 and $\langle\tau\rangle$ are shown in the ordinate. The red dotted line represents the trend of increasing relaxation time with increasing $\Delta\varepsilon$. A phonon dispersion spectrum for **Ni-BTT** is provided in Figure S5.

The computed elastic constants for the six coordination polymers are summarized in Table S4. The results show that the variation of organic π-conjugated spacers produces little changes on the C_{ii} of the linear coordination compounds (1.52×10^{-7} J m^{-3} for **Ni-BTT**, 1.57×10^{-7} J m^{-3} for **Ni-DMBTT**, 1.34×10^{-7} J m^{-3} for **Ni-DNBTT**, 1.49×10^{-7} J m^{-3} for **Ni-BQTT**, and 1.18×10^{-7} J m^{-3} for **Ni-ETT**). The elastic constants for linear compounds are around two times that of the zigzag structure ***z*-Ni-BTT** (0.80×10^{-7} J m^{-3}), which suggest that the ***z*-Ni-BTT** is less rigid. In addition, the calculated elastic constants are much larger than that of polyguanylic acid (4.36×10^{-10} J m^{-1})[39] but are comparable with those for graphdiyne nanoribbons ($1.66 - 2.99\times10^{-7}$ J m^{-1}).[40] Therefore, these ladder-like coordination polymers are much more rigid than polyguanylic acid but as rigid as graphdiyne nanoribbons.

The relaxation time for linear coordination polymers is found to decrease with the increment of $\Delta\varepsilon$ (Figure 4c). An observed trend is that the better the molecular orbital alignment, the smaller the DP, and eventually, the longer the relaxation time. Among the linear coordination polymers, **Ni-BTT** has the largest relaxation time of 4×10^5 fs due to its smallest DP constant (0.12 eV). Such large relaxation time is comparable to that of graphene nanoribbon, which reaches up to ~10^5 fs.[41] The relaxation time for **Ni-BQTT** (4×10^4 fs) is one magnitude smaller than that of **Ni-BTT** due to a slightly larger DP constant. The relaxation time of **Ni-DNBTT** (4×10^3 fs) and **Ni-DMBTT** (4×10^3 fs) are two orders of magnitude smaller than that of **Ni-BTT** due to moderate DP constants. **Ni-ETT** has the smallest relaxation time (40 fs) due to the largest DP constant (4.45 eV). These results imply that both **Ni-BTT** and **Ni-BQTT** should have excellent charge transport properties.

Intrinsic mobility.

The charge carrier mobility μ is a crucial measurable macroscopic quantity which determines the TE properties through the relation $\sigma = ne\mu$, where n, and e are the carrier concentration and elementary charge, respectively. At a given carrier concentration, the higher the mobility is, the higher the conductivity is. To obtain large mobility, a small effective mass and a long relaxation time are desirable, based on the relationship, $\mu = e < \tau > /m^*$. Since these coordination polymers have similar effective mass, the electron-phonon coupling plays a dominant role in their hole transport properties.

As shown in Figure 5, mobility increases almost linearly with the relaxation time. **Ni-BTT** has the largest relaxation time and the highest hole mobility (1.28×10^7 cm^2 V^{-1} s^{-1}) among the five linear coordination polymers due to its ultra-weak electron-phonon coupling. The hole mobility of **Ni-BQTT** (2.53×10^5 cm^2 V^{-1} s^{-1}) is two orders of magnitude smaller than that of **Ni-BTT** while larger than those of **Ni-DMBTT** (9.08×10^4 cm^2 V^{-1} s^{-1}), **Ni-DNBTT** (9.98×10^4 cm^2 V^{-1} s^{-1}), and **Ni-ETT** (8.40×10^2 cm^2 V^{-1} s^{-1}). In addition, our results suggest that the hole mobility of **Ni-BTT** is comparable to those for the graphene nanoribbons of ~ 10^6 cm^2 V^{-1} s^{-1}.[41] Meanwhile, the hole mobilities of **Ni-BQTT**, **Ni-DMBTT**, and **Ni-DNBTT** are similar to that of aromatic ring modulated carbon nanoribbon structures (10^4 cm^2 V^{-1} s^{-1}).[38] To the best of our knowledge, there is no direct mobility measurement of these coordination polymers. However, highly crystalline layered Cu-BHT (BHT = benzenehexathiol), a two-dimensional analog of **Ni-BTT**,[42] is highly conductive with extremely high electron and hole mobilities (99 cm^2 V^{-1} s^{-1} for holes and 116 cm^2 V^{-1} s^{-1} for electrons) at room temperature. A ladder-type Poly(p-Phenylenes) was found to have intrachain mobility close to 600 cm^2 V^{-1} s^{-1} at room temperature.[43] In compoarsion, these results coordination polymers investigated are predicted to posses higher intrinsic hole mobility.

TE properties predictions. Under rigid band approximation, the Seebeck coefficient and electrical conductivity can be presented as functions of carrier concentrations by varying the Fermi energy level. As an example, we plot the Seebeck coefficient, electrical conductivity, and power factor as a function of carrier concentration for **Ni-BTT** in Figure S9. The Seebeck coefficients decrease with the carrier concentrations, while the hole conductivity increases along with the carrier concentration. Consequently, a peak value of power factor ($(S^2\sigma)_{\max}$) appears at certain carrier concentration (e.g. 0.30×10^{20} cm^{-3} for **Ni-BTT**), which is commonly known as the optimal carrier concertation, N_{opt} for a TE material. For all the coordination polymers we studied, the

optimal electron concentrations are in the range of 10^{19} - 10^{20} cm^{-3}, which are feasible in experiment.[44] The Seebeck coefficients for the five linear coordination polymers at the corresponding N_{opt} are found to be at same order magnitude (in the range of 179 $\mu V\ K^{-1}$ – 214 $\mu V\ K^{-1}$), These values of Seebeck coefficients are close to that of the typical p-type poly(3,4-ethylenedioxythiophene) (70 $\mu V\ K^{-1}$ – 220 $\mu V\ K^{-1}$).[45][10]

A dramatic difference is observed for the hole conductivity which originates mostly from the large difference in the intrinsic hole mobility. **Ni-BTT** has the largest conductivity of 767 $\times 10^5$ S m^{-1} at its N_{opt} (0.30 $\times 10^{20}$ cm^{-3}) due to the largest intrinsic hole mobility. The conductivity of **Ni-BQTT** (σ = 173 $\times 10^5$ S m^{-1} at N_{opt} = 4.60 $\times 10^{20}$ cm^{-3}) is of the same magnitude but smaller than that of **Ni-BTT**. **Ni-DMBTT** (σ = 27.71 $\times 10^5$ S m^{-1} at N_{opt} = 1.61 $\times 10^{20}$ cm^{-3}) and **Ni-DNBTT** (σ = 7.50 $\times 10^5$ S m^{-1} at N_{opt} = 0.39 $\times 10^{20}$ cm^{-3}) have moderate conductivity while **Ni-ETT** (σ = 1.17$\times 10^5$ S m^{-1} at N_{opt} = 8.88 $\times 10^{20}$ cm^{-3}) is the poorest hole conductor at its N_{opt}. Although experimentally measured carrier concentrations are, so far, not yet available for these coordination polymers, a high room-temperature electron conductivity of up to 1580 S cm^{-1} was detected recently in highly crystalline Cu-BHT[42]. In addition, Heeger *et al.* have also demonstrated that high-quality polyacetylene films exhibit ultra-high hole conductivity of 10^4 -10^5 S cm^{-1} after doping with iodine at room temperature.[46] Compared with these experimental reports, our predicted conductivities for these coordination polymers are in the similar order of magnitude at their optimal doping.

With further analysis, the peak value of the power factor is found to increase with the mobility (Figure 5b), which can be explained by relation $(S^2\sigma)_{\max} = \frac{4{k_B}^2}{e}\mu \exp(\ln N_{\text{eff}} - 2)$ at optimal doping level.[35] At the optimal hole concentration, the power factor for the linear coordination polymers are in the range of 1- 3000$\times 10^5$ $\mu W\ m^{-1}\ K^{-2}$. Among them, **Ni-BTT** shows the best power factors (~ 10^8 $\mu W\ m^{-1}\ K^{-2}$) with the weak electron-phonon coupling (DP constant 0.12 eV) playing a key role. **Ni-BQTT** and **DMBTT** also show excellent power factors (~ 10^7 $\mu W\ m^{-1}\ K^{-2}$). The power factor of the **Ni-DNBTT** is on the order of magnitude of about ~10^6 $\mu W\ m^{-1}\ K^{-2}$ due to its moderate DP constant as compared with **Ni-BTT**. **Ni-ETT** have the lowest power factor (~ 10^5 $\mu W\ m^{-1}\ K^{-2}$) due to the largest DP constants. The $(S^2\sigma)_{\max}$ for ***z*-Ni-BTT** is 0.12$\times 10^6$ $\mu W\ m^{-1}\ K^{-2}$. In consideration of the difficulty in doping in experiments, we provide the TE transport coefficients at the hole concentrations up to ~ 10^{20} cm^{-3} in Figure S10. **Ni-BTT** still has high power factors at

all concentrations. The above discussions are only for p-type performance, for reader's reference, we have provided the n-type TE properties of this series of polymers in Table S5.

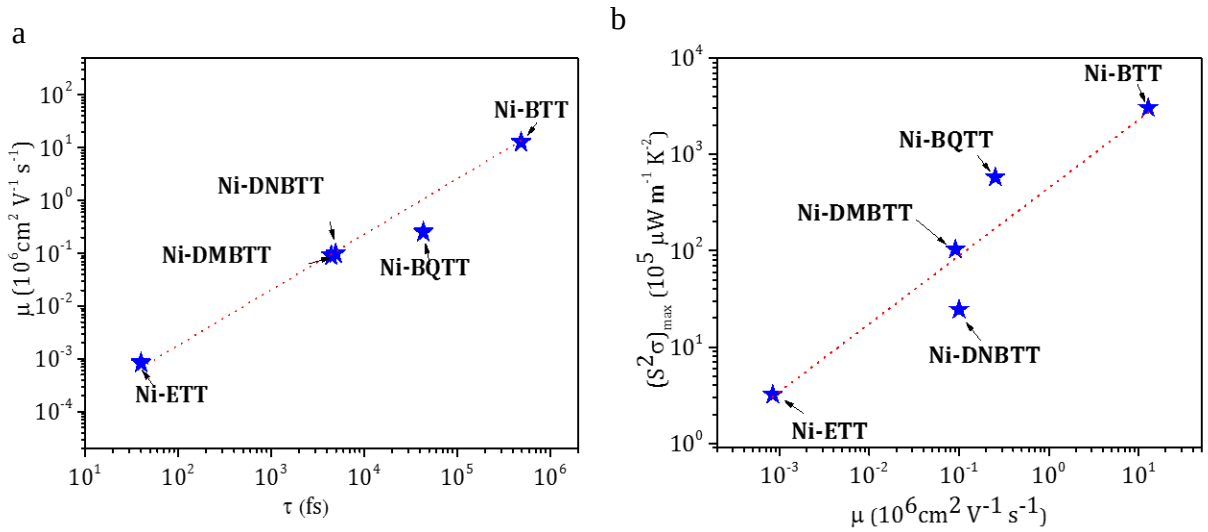

Figure 5. The correlation between p-type charge transport and TE properties on mean relaxation time at 298 K. (**a**) The relationship between the mobility, μ and mean relaxation time, $<\tau>$. The logarithmic mobility and mean relaxation time are shown in the ordinate and abscissa respectively. The red dotted line represents the trend of increasing mobility with increasing relaxation time. (**b**) The relationship between the peak value of power factor, $(S^2\sigma)_{max}$ and hole mobility, μ. The logarithmic maximum power factor and mean relaxation time are shown in the ordinate and abscissa respectively. The red dotted line represents the trend of increasing power factor with increasing mobility.

A screening rule.

Overall, our theoretical results show that the power factors are correlated with the molecular orbital alignment square planar nickel-tetrasulfide fragment and the π-conjugated spacer. An excellent frontier molecular orbital alignment results weakens the electron-phonon coupling (Figure 6). With suppressed electron-phonon coupling, the relaxation time is elevated, which leads to high

mobility and thereby high TE power factor. The route to reach high power factor is to eliminate the $\Delta\varepsilon$ between the frontier molecular orbitals of the fragments which comprise the coordination polymer. This requirement can be fulfilled by using different electron donating/withdrawing groups. In general, the use of electron-donating/withdrawing groups can rationally shift up/down of the molecular orbital energy levels of the fragment. Common electron-donating groups include alkane, and alkoxy groups while nitro groups and halogens are typical electron-withdrawing groups. In this work, since benzene and square planar nickel-tetrasulfide fragment have the best frontier molecular orbital alignment, **Ni-BTT** is found to exhibit the best TE power factor among the six coordination polymers investigated.

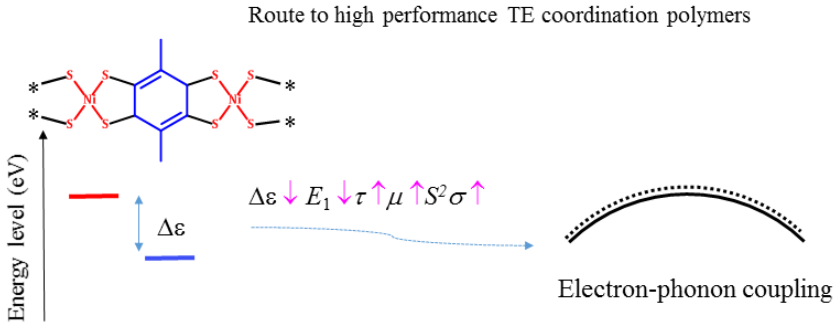

Figure 6. Schematic diagram of the proposed screening rules for high performance

Conclusions

In summary, an in-depth investigation of the geometry structure, electronic band structure, electron-phonon coupling, and TE properties have been carried out for a series of ladder-like highly rigid coordination polymers (**Ni-ETT**, **Ni-BTT**, **Ni-DMBTT**, **Ni-DNBTT**, **Ni-BQTT**, and ***z*-Ni-BTT**) using DFT calculations in combination with the Boltzmann transport theory. We discovered that the frontier molecular orbital alignment between the square planar nickel-tetrasulfide fragment and the organic π-conjugated is a strong predictor of TE power factor of the coordination polymers. With a suitable frontier molecular orbital alignment, the electron-phonon coupling is suppressed, enhancing the mobility and improving the TE power factor. We propose that an effective strategy to achieve high TE power factor is to minimize energy difference between the frontier molecular orbitals of the π-conjugated spacer and metal fragments. The energy level

of the π-conjugated spacer can be adjusted by introducing either electron-donating groups, *e.g.*, alkyl to increase its energy, or electron-withdrawing groups, *e.g*., nitro to decrease its energy. These results can be used as a powerful index to help experimentalists to rapidly screen the existing π-conjugated nickel coordination polymers for TE applications and design high-performance TE materials.

Acknowledgment

The authors would like to thanks the National Supercomputing Centre Singapore for providing the computing facility and the A*STAR Science and Engineering Research Council (SERC) of Singapore (1527200024 and 1527200019) for financial support.

References

[1] J. He, T.M. Tritt, *Science* . **2017**, *357*, 1369.

[2] L.E. Bell, *Science.* **2008**, *321*, 1457.

[3] F.J. DiSalvo, *Science* **1999**, *285*, 703.

[4] L.-D. Zhao, G. Tan, S. Hao, J. He, Y. Pei, H. Chi, H. Wang, S. Gong, H. Xu, V.P. Dravid, C. Uher, G.J. Snyder, C. Wolverton, M.G. Kanatzidis, *Science.* **2016**, *351*, 141.

[5] L.-D. Zhao, S.-H. Lo, Y. Zhang, H. Sun, G. Tan, C. Uher, C. Wolverton, V.P. Dravid, M.G. Kanatzidis, *Nature* **2014**, *508*, 373.

[6] C. Chang, M. Wu, D. He, Y. Pei, C.-F. Wu, X. Wu, H. Yu, F. Zhu, K. Wang, Y. Chen, L. Huang, J. Li, J. He, L. Zhao, *Science.* **2018**, *360*, 778.

[7] O. Bubnova, X. Crispin, *Energy Environ. Sci.* **2012**, *5*, 9345.

[8] Q. Zhang, Y. Sun, W. Xu, D. Zhu, *Adv. Mater.* **2014**, *26*, 6829.

[9] Z.U. Khan, J. Edberg, M.M. Hamedi, R. Gabrielsson, H. Granberg, L. WÃ¥gberg, I. Engquist, M. Berggren, X. Crispin, *Adv. Mater.* **2016**, *28*, 4556.

[10] O. Bubnova, Z.U. Khan, A. Malti, S. Braun, M. Fahlman, M. Berggren, X. Crispin, *Nat Mater* **2011**, *10*, 429.

[11] O. Bubnova, Z.U. Khan, H. Wang, S. Braun, D.R. Evans, M. Fabretto, P. Hojati-talemi, D. Dagnelund, J. Arlin, Y.H. Geerts, S. Desbief, D.W. Breiby, J.W. Andreasen, R. Lazzaroni, W.M. Chen, I. Zozoulenko, M. Fahlman, P.J. Murphy, M. Berggren, X. Crispin, *Nat. Mater.* **2013**, *13*, 1.

[12] H. Wang, J.-H. Hsu, S.-I. Yi, S.L. Kim, K. Choi, G. Yang, C. Yu, *Adv. Mater.* **2015**, *27*, 6855.

[13] C. Meng, C. Liu, S. Fan, *Adv. Mater.* **2010**, *22*, 535.

[14] B.T. McGrail, A. Sehirlioglu, E. Pentzer, *Angew. Chemie - Int. Ed.* **2015**, *54*.

[15] Y. Sun, P. Sheng, C. Di, F. Jiao, W. Xu, D. Qiu, D. Zhu, *Adv. Mater.* **2012**, *24*, 932.

[16] Y. Sun, L. Qiu, L. Tang, H. Geng, H. Wang, F. Zhang, D. Huang, W. Xu, P. Yue, Y. Guan, F. Jiao, Y. Sun, D. Tang, C. Di, Y. Yi, D. Zhu, *Adv. Mater.* **2016**, *28*, 3351.

[17] J.-H. Dou, L. Sun, Y. Ge, W. Li, C.H. Hendon, J. Li, S. Gul, J. Yano, E.A. Stach, M. Dincă, *J. Am. Chem. Soc.* **2017**, *139*, 13608.

[18] R. Matsuoka, R. Sakamoto, T. Kambe, K. Takada, T. Kusamoto, H. Nishihara, *Chem. Commun.* **2014**, *50*, 8137.

[19] J.P. Perdew, K. Burke, M. Ernzerhof, *Phys. Rev. Lett.* **1996**, *77*, 3865.

[20] J. Heyd, G.E. Scuseria, M. Ernzerhof, *J. Chem. Phys.* **2003**, *118*, 8207.

[21] S. Grimme, J. Antony, S. Ehrlich, H. Krieg, *J. Chem. Phys.* **2010**, *132*, 154104.

[22] B. Liu, W. Qiao, Z.Y. Wang, *RSC Adv.* **2015**, *5*, 6815.

[23] S. de Gironcoli, *Phys. Rev. B* **1995**, *51*, 6773.

[24] C.L. Fu, K.M. Ho, *Phys. Rev. B* **1983**, *28*, 5480.

[25] M. Gajdoš, K. Hummer, G. Kresse, J. Furthmüller, F. Bechstedt, *Phys. Rev. B* **2006**, *73*, 045112.

[26] M. Hutchinson, M. Widom, *Comput. Phys. Commun.* **2011**, *183*, 1422.

[27] P.E. Blöchl, *Phys. Rev. B* **1994**, *50*, 17953.

[28] A.A. Mostofi, J.R. Yates, G. Pizzi, Y.S. Lee, I. Souza, D. Vanderbilt, N. Marzari, *Comput. Phys. Commun.* **2014**, *185*, 2309.

[29] G.K.H. Madsen, D.J. Singh, *Comput. Phys. Commun.* **2006**, *175*, 67.

[30] G.K.H. Madsen, *J. Am. Chem. Soc.* **2006**, *128*, 12140.

[31] J. Bardeen, W. Shockley, *Phys. Rev.* **1950**, *80*, 72.

[32] J. Ochocki, P. Chaudhuri, W.L. Driessen, R.A.G. De Graaf, F.B. Hulsbergen, J. Reedijk, *Inorganica Chim. Acta* **1990**, *167*, 15.

[33] X. Yao, J. Wang, G. Wu, S.S. Goh, H. Zhu, S.-W. Yang, *J. Mater. Chem. C* **2017**, *5*, 3585.

[34] B.B.-Y.Y. Hsu, C.-M.M. Cheng, C. Luo, S.N. Patel, C. Zhong, H. Sun, J. Sherman, B.H. Lee, L. Ying, M. Wang, G. Bazan, M. Chabinyc, J.L. Brédas, A. Heeger, *Adv. Mater.* **2015**, *27*, 7759.

[35] S.-W. Shi, Wen; Wu, Gang; Xue, Yong; Wang, Jian-Sheng; Zheng, Jin-Cheng; Deng, Tianqi; Xu, Jianwei; Yang, *J Am Chem Soc* **n.d.**

[36] P.-A. Mante, C.C. Stoumpos, M.G. Kanatzidis, A. Yartsev, *Nat. Commun.* **2017**, *8*, 14398.

[37] L.P. Tang, L.M. Tang, H. Geng, Y.P. Yi, Z. Wei, K.Q. Chen, H.X. Deng, *Appl. Phys. Lett.* **2018**, *112*, 1.

[38] Q. Ai, K. Jarolimek, S. Mazza, J.E. Anthony, C. Risko, *Chem. Mater.* **2018**, *30*, 947.

[39] F.B. Beleznay, F. Bogar, Z. Szekeres, J. Ladik, *J. Chem. Phys.* **2006**, *124*.

[40] M. Long, L. Tang, D. Wang, Y. Li, Z. Shuai, *ACS Nano* **2011**, *5*, 2593.

[41] M.-Q. Long, L. Tang, D. Wang, L. Wang, Z. Shuai, *J. Am. Chem. Soc.* **2009**, *131*, 17728.

[42] X. Huang, P. Sheng, Z. Tu, F. Zhang, J. Wang, H. Geng, Y. Zou, C. Di, Y. Yi, Y. Sun, W. Xu, D. Zhu, *Nat. Commun.* **2015**, *6*, 7408.

[43] P. Prins, F.C. Grozema, J.M. Schins, S. Patil, U. Scherf, L.D.A. Siebbeles, *Phys. Rev. Lett.* **2006**, *96*, 1.

[44] D. Huang, C. Wang, Y. Zou, X. Shen, Y. Zang, H. Shen, X. Gao, Y. Yi, W. Xu, C. Di, D.

Zhu, *Angew. Chemie Int. Ed.* **2016**, *55*, 10672.

[45] W. Shi, T. Zhao, J. Xi, D. Wang, Z. Shuai, *J. Am. Chem. Soc.* **2015**, *137*, 12929.

[46] N. Basescu, Z.-X. Liu, D. Moses, A.J. Heeger, H. Naarmann, N. Theophilou, *Nature* **1987**, *327*, 403.